Available online at www.sciencedirect.com
ScienceDirect
Nuclear Physics B Proceedings Supplement 00 (2014) 1–8
Nuclear Physics B Proceedings Supplement

# Measurement of Higgs boson couplings at the International Linear Collider

Junping Tian[1], Keisuke Fujii[1]

*High Energy Accelerator Research Organization (KEK), Oho 1-1, 305-0801, Tsukuba, Japan*

**Abstract**

Precision measurement of Higgs boson couplings will be the central task of high energy physics in the next decades, as the key to the unknown. This article gives an overview of how various Higgs couplings will be measured at the International Linear Collider (ILC). Emphases are placed on the ILC's capability of performing fully model independent determination of absolute $HZZ$ and $HWW$ couplings, the Higgs total width, and hence various other Higgs couplings, such as $Hbb$ and $Hcc$, which cover essentially all the crucial ones including the top-Yukawa coupling $Htt$ and the self-coupling $\lambda_{HHH}$. The strategy to get the best precision measurements at the ILC is through staged running. A method of global fitting is applied to utilize all of the available information from each stage and to derive combined precisions.

*Keywords:* Higgs couplings, ILC, Electroweak Symmetry Breaking

## 1. Introduction

After the spectacular discovery of a 125 GeV Higgs boson [1, 2], a central question is whether this Higgs boson is the one predicted by the Standard Model (SM) where the couplings of the Higgs boson to SM particles and itself (self-coupling) are uniquely determined once the particles in question as well as the Higgs boson mass are given. Precision measurements of Higgs couplings are no doubt the key to questing that answer. On the other hand, the dynamics behind the electroweak symmetry breaking (EWSB) remains unknown. The only explanation of the EWSB in the SM is by requiring $\mu^2 < 0$ in the Higgs potential. We believe this puzzle will be unravelled by physics beyond the SM (BSM), such as the proposed super symmetry (SUSY) or Composite Higgs Model, where the $\mu^2$ can be computed by first principle and naturally run to negative value at electroweak scale [3], as shown schematically in Fig.1. However we don't yet know exactly the energy scale to search those new physics, except that the scale would be around TeV which is suggested by the well-known naturalness or hierarchy problem [4] and other theoretical considerations. But it is expected that BSM contributions will cause the Higgs boson couplings deviate from their SM values. The size of the deviations depends on new physics scale, which is well explained in Haber's Decoupling Limit, $\Delta g \sim \frac{m_H^2}{M^2}$, where $\Delta g$ is deviation of Higgs coupling, $m_H$ is the mass of Higgs boson and $M$ is the mass scale of new heavy particles in the BSM models. Therefore the newly discovered Higgs boson provides a unique window to uncover the BSM physics and next energy scale by studying this particle in detail. Figure 2 gives examples of deviations of various Higgs couplings in the MSSM (left) and MCHM5 (right) models [5], showing us two general features of new physics models that firstly the deviations of couplings are small at the level of a few percent, secondly the patterns of deviations for all couplings among models are different. An experimental program which can provide both precision at the required level as well as complete coverage of all Higgs couplings is needed to identify the nature of new physics in addition to discovering it.

The International Linear Collider (ILC), with $\sqrt{s}$ =

[1] on behalf of the ILC physics and detector study

200 – 500 GeV upgradable to 1 TeV, is the precision machine to study every detail of the Higgs particle. The technical design report (TDR) [6, 7] of the ILC has been delivered. The detailed baseline design (DBD) [8] of the two proposed detectors, ILD and SiD with a push-pull scheme, has also been completed. The physics reach based on the performance of the designed accelerator and detectors is fully discussed in the physics volume of the TDR [5]. This article gives a brief introduction to how the measurements of Higgs couplings are performed at the ILC. Emphasises are placed on some unique features at the ILC, such as model independent determinations of $HZZ$ and $HWW$ couplings and Higgs total width, capabilities of $H \to c\bar{c}$ and $H \to$ invisible search, direct probe of top-Yukawa coupling and Higgs self-coupling. More comprehensive review of the Higgs physics at the ILC is available in the ILC Higgs White Paper [9] which was prepared for the Snowmass process 2013.

A staged running program of the ILC is proposed to make optimal use of the available physics channels at different collision energies. The major Higgs production processes are shown in Fig.3 and 4, and their cross sections as a function of $\sqrt{s}$ are shown in Fig.5. At 250 GeV where Higgs-strahlung process $ZH$ reaches its maximum cross section, $HZZ$ coupling and various Higgs branching ratios will be well measured, as well as Higgs profile such as spin, CP and mass. At 350 GeV, a threshold scan of top quark pair production, with precise measurements of a well-defined top quark mass and the forward-backward asymmetry $A_{\rm FB}$, complements the Higgs program, where the measurement of the total Higgs width benefits from the turn-on of the $\nu\bar{\nu}H$ process via $WW$-fusion. At 500 GeV, firstly cross section of $WW$-fusion process is significantly larger which provides precision determination of $HWW$ coupling and Higgs total width; secondly also most importantly it opens the direct production of $t\bar{t}H$ for top-Yukawa coupling measurement, and $ZHH$ production for Higgs self-coupling measurement. At 1 TeV, many more Higgs events will be collected by $\nu\bar{\nu}H$ production via $WW$-fusion, hence it allows better measurement of Higgs rare decay modes, such as $H \to \gamma\gamma$ and $H \to \mu^+\mu^-$; Higgs self-coupling will be significantly improved by using double Higgs production process $\nu\bar{\nu}HH$ via $WW$-fusion; it will also improve top-Yukawa coupling due to much larger cross section of $t\bar{t}H$. The integrated luminosities assumed at each stage are 250 fb$^{-1}$ at 250 GeV, 500 fb$^{-1}$ at 500 GeV, and 1000 fb$^{-1}$ at 1 TeV, which are the nominal values in the baseline design. There is also feasibility of luminosity upgrade [9], which provides 1150 fb$^{-1}$ at 250 GeV, 1600 fb$^{-1}$ at 500 GeV, and 2500 fb$^{-1}$ at 1 TeV. According to the TDR, the electron beam can be polarized to 80% at all energies; the positron beam can be polarized to 30% at 250 – 500 GeV and to 20% at 1 TeV. The beam polarization is actually a very powerful tool to enhance the cross section of Higgs production. Here $P(e^-, e^+) = (-80\%, +30\%)$ is assumed at 250 – 500 GeV, and $P(e^-, e^+) = (-80\%, +20\%)$ is assumed at 1 TeV. In the following sections, measurement of each Higgs coupling will be explained, and results based on full detector simulation will be delivered.

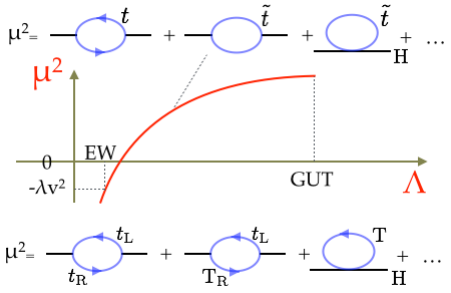


Figure 1: A schematic view of running of $\mu^2$ together with the Feynman diagrams in SUSY (top) and Little Higgs Model (bottom) to compute the $\mu^2$.

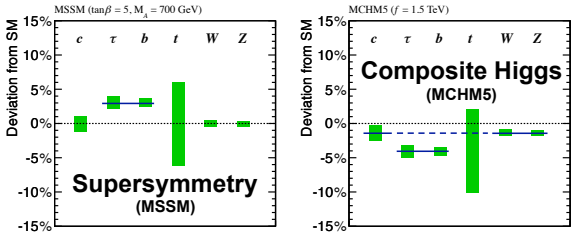


Figure 2: Expected deviations of Higgs couplings in MSSM (left) and MCHM5 (right).

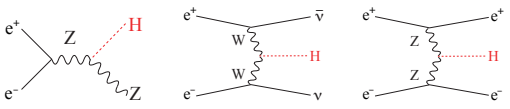


Figure 3: Feynman diagrams of major Higgs production processes at the ILC: Higgs-strahlung $e^+e^- \to ZH$ (left), $WW$-fusion $e^+e^- \to \nu\bar{\nu}H$ (middle) and $ZZ$-fusion $e^+e^- \to e^+e^-H$ (right).

## 2. $HZZ$ coupling

The well defined four-momentum of the initial state ($p_{CM}$) at the ILC allows an inclusive measurement of

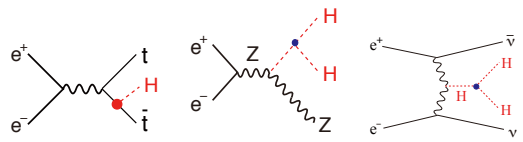


Figure 4: Feynman diagrams with top-Yukawa coupling and Higgs self-coupling processes at the ILC: $e^+e^- \to t\bar{t}H$ (left), $e^+e^- \to ZHH$ (middle) and $e^+e^- \to \nu\bar{\nu}HH$ via $WW$-fution (right).

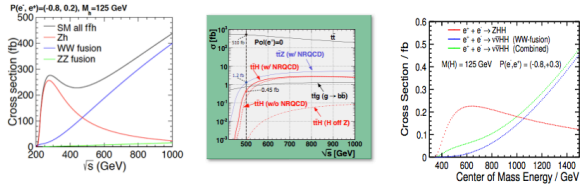


Figure 5: Cross sections of the major Higgs production processes as a function of $\sqrt{s}$: $e^+e^- \to ZH$, $e^+e^- \to \nu\bar{\nu}H$ and $e^+e^- \to e^+e^-H$ (left); $e^+e^- \to t\bar{t}H$ (middle); $e^+e^- \to ZHH$ and $e^+e^- \to \nu\bar{\nu}HH$ (right).

the cross section of $e^+e^- \to ZH$. Without looking into Higgs decays, as long as we can reconstruct the four-momentum of the $Z$ boson ($p_Z$), the Higgs four-momentum, hence invariant mass ($M_X$), can be calculated by the recoil technique, $M_X = \sqrt{p_{CM}^2 - p_Z^2}$. The most effective and precise way to reconstruct $p_Z$ is using the leptonic decay of $Z \to l^+l^-$, $l = e$ or $\mu$. Experimentally we only need to find a lepton pair with an invariant mass consistent with the $Z$ mass and then the recoil mass of the lepton pair is given by $M_X = \sqrt{p_{CM}^2 - (p_{l^+} + p_{l^-})^2}$, as shown in Fig.6 [10, 11]. By fitting the recoil mass distribution with signal and background components, we get the total cross section of $e^+e^- \to ZH$ ($\sigma_{ZH}$) since the branching ratios of $Z \to l^+l^-$ are precisely known. From the sharp peak of the recoil mass distribution, Higgs mass can be precisely determined, $\Delta m_H \sim 30$ MeV with baseline integrated luminosity. From the measured $\sigma_{ZH}$, the coupling $g_{HZZ}$ can be extracted fully model-independently based on $Y_1 := \sigma_{ZH} = F_1 g_{HZZ}^2$, where factor $F_1$ can be calculated unambiguously for the Feynman diagram in Fig.3 (left) and $Y_i$ always denotes observable in this article, which is

$$g_{HZZ} = \sqrt{\frac{Y_1}{F_1}}.$$

The expected precisions of $g_{HZZ}$ for $m_H = 125$ GeV at $\sqrt{s} = 250$ GeV and 500 GeV are shown in Table 1. Obviously the two crucial factors in this measurement are precisely known beam condition for initial state and high momentum resolution for the lepton reconstruction.

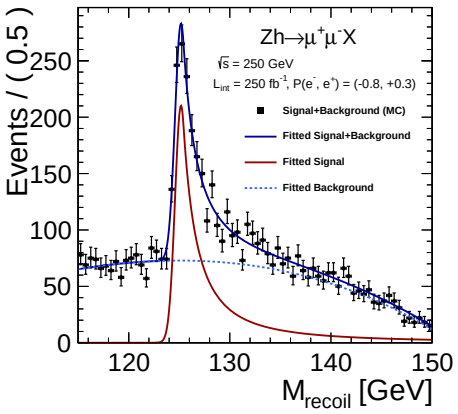


Figure 6: Recoil mass distribution of $e^+e^- \to ZH$ followed by $Z \to \mu^+\mu^-$ at 250 GeV with a Higgs mass of 125 GeV.

An alternative approach to reconstruct $p_Z$ is the hadronic decay of $Z \to q\bar{q}$. However, it's not very trivial that the reconstruction of $Z$ from 2-jets will not be affected by Higgs decay products. But since branching ratio of $Z \to q\bar{q}$ is much larger than leptonic mode, there's great benefit to pursue this approach. There are lots of efforts ongoing, essentially to carefully categorize event selection to get similar efficiencies for different Higgs decay modes [12, 13, 14]. At 500 GeV, the measurement will be easier because both the $Z$ and $H$ bosons are sufficiently boosted, which makes their decay products better separated [15]. At 250 GeV and 350 GeV, current analyses suggest that it's also very promising to get systematic error well controlled. In this article we only include 500 GeV hadronic recoil measurements in the global fitting.

Overall, the recoil mass measurement using $Z \to l^+l^-$ is one of the flagship measurements at the ILC, which gives the absolute $HZZ$ coupling in a fully model independent way, and is the key to unlock all other couplings. And clearly the best energy for this measurement is 250 GeV, where $\sigma_{ZH}$ reaches its maximum and the momentum resolution is the highest.

## 3. *HWW* coupling

The $WW$-fusion process $e^+e^- \to \nu\bar{\nu}H$ is employed to measure the $HWW$ coupling ($g_{HWW}$), because its cross section $\sigma_{\nu\bar{\nu}H}$ is proportional to $g_{HWW}^2$. Unlike the case of $e^+e^- \to ZH$ the final state neutrinos cannot be directly reconstructed by the detector and hence the recoil technique is not applicable any more. We hence need to rely on some exclusive Higgs decay. Here we take

advantage of the decay mode with the largest branching ratio: $e^+e^- \to \nu\bar{\nu}H \to \nu\bar{\nu}b\bar{b} \sim 57.8\%$, where the relevant observable is $Y_2 := \sigma_{\nu\bar{\nu}H} \times \mathrm{Br}(H \to b\bar{b}) = F_2 \cdot g^2_{HWW} \cdot \mathrm{Br}(H \to b\bar{b})$. To extract $g_{HWW}$, we first need to know $\mathrm{Br}(H \to b\bar{b})$. This is measured using the process $e^+e^- \to ZH \to Zb\bar{b}$ [16], where the observable is $Y_3 := \sigma_{ZH} \times \mathrm{Br}(H \to b\bar{b}) = F_3 \cdot g^2_{HZZ} \cdot \mathrm{Br}(H \to b\bar{b})$. From the ratio of $Y_2/Y_3$, we can obtain the ratio of $g_{HWW}/g_{HZZ}$ and further extract $g_{HWW}$, which is

$$g_{HWW} = \sqrt{\frac{Y_1 Y_2}{Y_3}\frac{F_3}{F_1 F_2}}.$$

The observables $Y_1$ and $Y_2$ based on the Higgs-strahlung process are well measured at 250 GeV. However, $Y_2$ based on the $WW$-fusion process is limited by its small cross section $\sim$ 14fb at 250 GeV as shown in Fig.5 (left). At 500 GeV, the cross section of the $WW$-fusion process is one order-of-magnitude larger $\sim$ 149fb, which allows a precision measurement of $Y_2$. Figure 7 shows the reconstructed missing mass at 250 GeV (left) and invariant mass of the Higgs candidates at 500 GeV (right) in the analysis of $e^+e^- \to \nu\bar{\nu}H$, followed by $H \to b\bar{b}$ [17], where it's clearly seen $WW$-fusion process can be measured significantly better at higher energies. The expected precisions of $g_{HWW}$ at $\sqrt{s}$ = 250 GeV and 500 GeV are shown in Table 1. Conclusion here is that the absolute $HWW$ coupling can be extracted model independently and going to higher energy is crucial to get the precision of $g_{HWW}$ as good as $g_{HZZ}$.

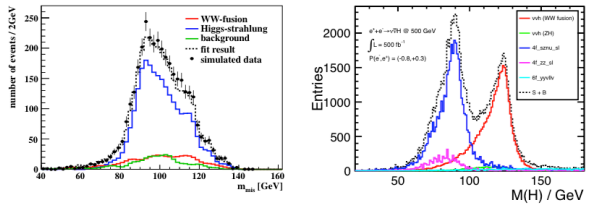


Figure 7: Reconstructed missing mass at 250 GeV (left) and invariant mass of Higgs at 500 GeV (right) in the analysis of $e^+e^- \to \nu\bar{\nu}H$, followed by $H \to b\bar{b}$.

## 4. Higgs total width $\Gamma_H$

At the ILC the Higgs total width ($\Gamma_H$) can be determined model independently by the partial width of the Higgs to $ZZ^*$ ($\Gamma_{H\to ZZ^*}$) decay divided by the branching ratio of $H \to ZZ^*$, $\Gamma_H = \frac{\Gamma_{H\to ZZ^*}}{\mathrm{Br}(H\to ZZ^*)}$. The partial width $\Gamma_{H\to ZZ^*}$ can be calculated with the well measured $g_{HZZ}$. But $\mathrm{Br}(H \to ZZ^*)$ is rather statistically limited by its small branching ratio $\sim$ 2.7%. Since $\mathrm{Br}(H \to WW^*)$ is much larger, $\sim$ 22%, a better way is correspondingly by $\Gamma_H = \frac{\Gamma_{H\to WW^*}}{\mathrm{Br}(H\to WW^*)}$, where $\Gamma_{H\to WW^*}$ can be calculated with $g_{HWW}$. An interesting observable here is $Y_4 := \sigma_{\nu\bar{\nu}H} \times \mathrm{Br}(H \to WW^*) = F_4 \cdot \frac{g^4_{HWW}}{\Gamma_H}$, which together with known $g_{HWW}$ gives,

$$\Gamma_H = \frac{F_4}{Y_4} \cdot g^4_{HWW} = \frac{Y_1^2 Y_2^2}{Y_3^2 Y_4}\frac{F_3^2 F_4}{F_1^2 F_2^2}.$$

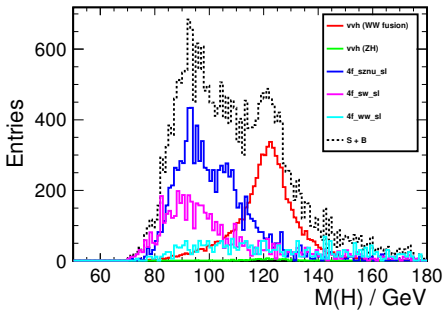


Figure 8: Reconstructed invariant mass of Higgs at 500 GeV in the analysis of $e^+e^- \to \nu\bar{\nu}H$, followed by $H \to WW^*$.

Figure 8 (right) shows the reconstructed invariant mass of the Higgs candidates in the analysis of $e^+e^- \to \nu\bar{\nu}H$, followed by $H \to WW^*$ at 500 GeV [17]. Obviously for better determination of the Higgs total width one needs higher energy. It is also worth emphasizing that eventually the precisions of $2\frac{\Delta Y_1}{Y_1}$ and $\frac{\Delta Y_4}{Y_4}$ will limit the precision of the total width, since $Y_3$ usually is better measured than $Y_1$, and $Y_2$ is twice better than $Y_4$. The expected precisions of $\Gamma_H$ at different energies are shown in Table 1.

## 5. Higgs couplings to $bb$, $cc$ and $gg$

The clean environment at the ILC allows efficient identification of a $b-$jet, $c-$jet or light quark jet, and discrimination of $H \to b\bar{b}$, $H \to c\bar{c}$ and $H \to gg$ events over background events. The measurement is performed by first selecting events where Higgs can be reconstructed from two jets, taking into account both $ZH$ and $\nu\bar{\nu}H$ productions and various $Z$ decay modes. Then both jets from Higgs are tagged with a likeness of $b-$jet or $c-$jet by flavor tagging tool LCFIPlus [18], and the likenesses of two jets are summed to one likeness for each event. Figure 9 shows the 2D pattern of b-likeness versus c-likeness for various types of events, including signal $e^+e^- \to ZH$ followed by $H \to b\bar{b}$, $H \to c\bar{c}$ and $H \to gg$ events, $e^+e^- \to ZH$ followed by other Higgs decays events, and the SM background events. As

clearly seen, $H \to b\bar{b}$, $H \to c\bar{c}$ and $H \to gg$ events are distinguishable. The number of events for each category is obtained from a simultaneous fit to template histograms. The direct observables in this measurement are $\sigma_{ZH} \times \mathrm{Br}(H \to b\bar{b})$, $\sigma_{ZH} \times \mathrm{Br}(H \to c\bar{c})$ and $\sigma_{ZH} \times \mathrm{Br}(H \to gg)$, which are proportional to $\frac{g^2_{HZZ}g^2_{Hbb}}{\Gamma_H}$, $\frac{g^2_{HZZ}g^2_{Hcc}}{\Gamma_H}$ and $\frac{g^2_{HZZ}g^2_{Hgg}}{\Gamma_H}$. Once $g_{HZZ}$ and $\Gamma_H$ are known, couplings $Hbb$, $Hcc$ and $Hgg$ can be determined, of which precisions are shown in Table 1.

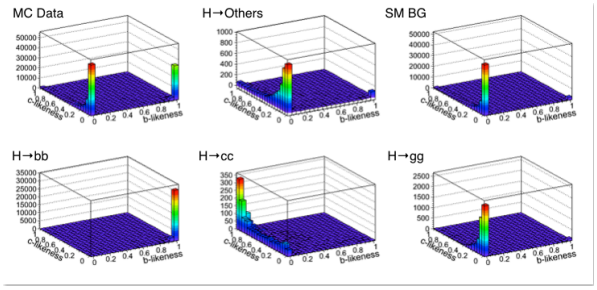


Figure 9: 2D pattern of b-likeness versus c-likeness for various types of events, including signal $e^+e^- \to ZH$ followed by $H \to b\bar{b}$, $H \to c\bar{c}$ and $H \to gg$ events (three figures in the bottom), $e^+e^- \to ZH$followed by other Higgs decays events (top-middle), the SM background events (top-right), and all events together (top-left).

## 6. Higgs invisible decay

Measurement of invisible Higgs decays can be performed also using recoil technique in process $e^+e^- \to ZH$ followed by $Z \to l^+l^-$ or $Z \to q\bar{q}$. Since here Higgs decays invisibly, there's no ambiguity to reconstruct Z, hence hadronic decay of Z will be the dominant contribution. Figure 10 shows the recoil mass distribution of $e^+e^- \to ZH$ events followed by $Z \to q\bar{q}$ and Higgs to invisible, together with background events, assuming branching ratio of Higgs invisible decay is 10% [19]. A peak from Higgs invisible decay can be clearly observed. The up limit of Higgs invisible branching ratio can be determined to 0.95% within 95% confidence level with baseline integrated luminosities which is again completely model independent.

## 7. Higgs couplings to $\tau\tau$, $\gamma\gamma$ and $\mu\mu$

At the ILC Higgs to $\tau\tau$ can be well reconstructed by some sophisticated TauFinder [20], and more importantly the missing neutrinos in those two $\tau$ can be recovered by collinear approximation thanks to known initial states which helps a lot to separate signal with $Z \to \tau\tau$ events as shown in Fig. 11. For $H \to \gamma\gamma$ and

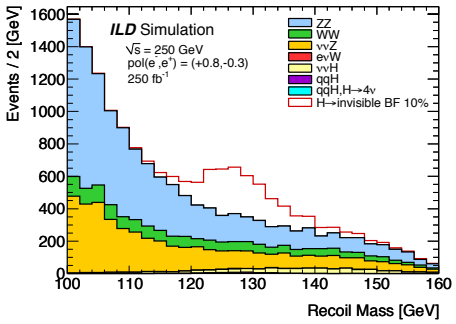


Figure 10: The recoil mass distribution of $e^+e^- \to ZH$ events followed by $Z \to q\bar{q}$ and Higgs to invisible (red), together with background events, assuming branching ratio of Higgs invisible decay is 10%.

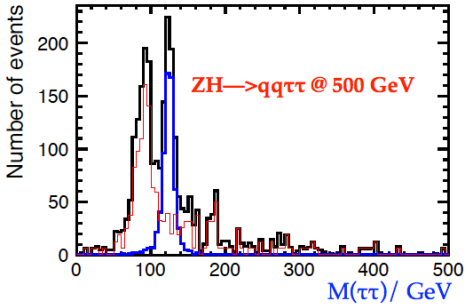


Figure 11: The reconstructed invariant mass of $\tau^+\tau^-$ distribution of $e^+e^- \to ZH$ events followed by $Z \to q\bar{q}$ and $H \to \tau^+\tau^-$ (blue), together with background events (red) dominanted by $e^+ + e^- \to ZZ \to q\bar{q}\tau^+\tau^-$ by collinear approximation.

$H \to \mu^+\mu^-$, measurements are very straightforward since isolated $\gamma$ and $\mu$ are really easy to reconstruct. The measurements are only limited by the statistics since branching ratios of these two modes are really small. Nevertheless at 1 TeV ILC, we can measure these two modes relatively well [21, 22], as shown in Fig. 12. It's worth mentioning here that there's great synergy between LHC and ILC measurements for $H \to \gamma\gamma$. At the LHC, available statistics of $H \to \gamma\gamma$ events is much higher, but only ratio of $\mathrm{Br}(H \to ZZ^*)$ and $\mathrm{Br}(H \to \gamma\gamma)$, which is proportional to ratio of $g^2_{HZZ}$ and $g^2_{H\gamma\gamma}$, can be well measured. By combining that ratio with precision $HZZ$ coupling measurement at the ILC, we can significantly improve the precision of $H\gamma\gamma$ coupling [23].

## 8. Top-Yukawa coupling $Htt$ and Higgs self-coupling $\lambda_{HHH}$

The largest Yukawa coupling, top-Yukawa coupling, can be directly accessed at the ILC through the process

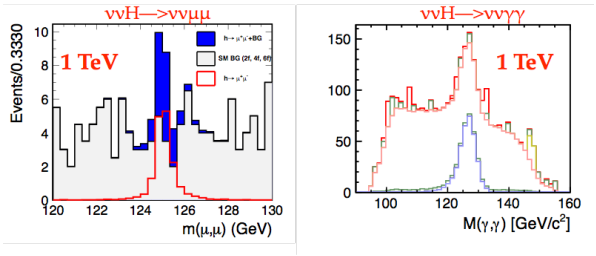


Figure 12: Left: the reconstructed invariant mass of $\mu^+\mu^-$ distribution of $e^+e^- \to \nu\bar{\nu}H$ events followed by $H \to \mu^+\mu^-$, together with background events dominanted by $e^+ + e^- \to \nu\bar{\nu}Z \to \nu\bar{\nu}\mu^+\mu^-$; right: the reconstructed invariant mass of $\gamma\gamma$ distribution of $e^+e^- \to \nu\bar{\nu}H$ events followed by $H \to \gamma\gamma$, together with background events dominanted by $e^+ + e^- \to \nu\bar{\nu}\gamma\gamma$.

$e^+e^- \to t\bar{t}H$. The force which makes vacuum condense, the Higgs self-coupling, can be measured through double Higgs production processes $e^+e^- \to ZHH$ and $e^+e^- \to \nu\bar{\nu}HH$. The details of these two analyses are available in another article of this proceedings [24]. Both of these two measurement are challenging at the ILC due to small cross sections and complicated final states. And there are important physics issues, such as QCD bound state effect in $t\bar{t}H$ at 500 GeV and interference effect in both $ZHH$ and $\nu\bar{\nu}HH$. Please refer that article [24] and also original analyses [25, 26, 27, 28, 29]. Here only the results are shown in Table 1.

## 9. Global fit

Staged running and various production processes provide many independent $Y_i = \sigma \times \mathrm{Br}(H \to XX)$ measurements with error $\Delta Y_i$ [9], each of which can be predicted by $Y_i' = F_i \cdot \frac{g_{HZZ}^2 g_{HXX}^2}{\Gamma_H}$, or $Y_i' = F_i \cdot \frac{g_{HWW}^2 g_{HXX}^2}{\Gamma_H}$, or $Y_i' = F_i \cdot \frac{g_{Htt}^2 g_{HXX}^2}{\Gamma_H}$, where $XX$ means some specific Higgs decay mode and $F_i$ is some calculable factor corresponding to the search mode. In addition, the recoil mass measurements provide absolute cross section measurements of the $e^+e^- \to ZH$, process, which can be predicted as $Y_j' = F_j \cdot g_{HZZ}^2$. To combine all of these measurements to exact the 9 couplings, $HZZ$, $HWW$, $Hbb$, $Hcc$, $Hgg$, $H\tau\tau$, $H\mu\mu$, $Htt$, and $H\gamma\gamma$, and the Higgs total width, $\Gamma_H$, a method of model independent global fit is applied by constructing a $\chi^2$ which is defined as following:

$$\chi^2 = \sum_{i=1}^{i=N} \left(\frac{Y_i - Y_i'}{\Delta Y_i}\right)^2,$$

where $Y_i$ is the measured value, $\Delta Y_i$ is the error on $Y_i$, $N$ is the total number of measurements and $Y_i'$ is the predicted value which can always be parameterized by couplings and Higgs total width. Next step is to minimize this $\chi^2$ and get the fitted values of the 10 parameters and their errors. Here we assume all the 9 couplings and the Higgs total width are free parameters without any correlation. The result of our global fit is given in Table 1, at different energies and for both baseline and luminosity upgraded scenarios. The systematic errors of luminosity, beam polarisations and $b$-tag efficiencies are included in global fit [9], but theoretical errors are not considered here, which however will be well controlled to below sub-percent level at the time of ILC running [30].

The global fit based on above strategy is completely model independent. Because $HZZ$ coupling precision limited all other precisions, in future if we could include hadronic recoil measurement at 250 GeV, all the precisions would be improved. In addition, it is suggested that we may constrain the sum of all branching ratio to 1 [31], by which the results will be improved by another factor of 2.

| $\Delta g/g$ | Baseline | | | LumiUP | | |
|---|---|---|---|---|---|---|
| | 250 GeV | +500 GeV | +1 TeV | 250 GeV | +500 GeV | +1 TeV |
| $\int Ldt$/fb | 250 | 500 | 1000 | 1150 | 1600 | 2500 |
| $g_{HZZ}$ | 1.3% | 1.0% | 1.0% | 0.61% | 0.51% | 0.51% |
| $g_{HWW}$ | 4.8% | 1.2% | 1.1% | 2.3% | 0.58% | 0.56% |
| $g_{Hbb}$ | 5.3% | 1.6% | 1.3% | 2.5% | 0.83% | 0.66% |
| $g_{Hcc}$ | 6.8% | 2.8% | 1.8% | 3.2% | 1.5% | 1.0% |
| $g_{Hgg}$ | 6.4% | 2.3% | 1.6% | 3.0% | 1.2% | 0.87% |
| $g_{H\tau\tau}$ | 5.7% | 2.3% | 1.7% | 2.7% | 1.2% | 0.93% |
| $g_{H\gamma\gamma}$ | 18% | 8.4% | 4.0% | 8.2% | 4.5% | 2.4% |
| $g_{H\mu\mu}$ | - | - | 16% | - | - | 10% |
| $g_{Htt}$ | - | 14% | 3.1% | - | 7.8% | 1.9% |
| $\Gamma_H$ | 11% | 5.0% | 4.6% | 5.4% | 2.5% | 2.3% |
| Inv. | 0.95% | 0.95% | 0.95% | 0.44% | 0.44% | 0.44% |
| $\lambda_{HHH}$ | - | 83% | 21% | - | 46% | 13% |

Table 1: Expected precisions of Higgs couplings, total Higgs width, up limit of invisible branching ratio (95% C.L.) and Higgs self-coupling for both baseline and luminosity upgrade (LumiUP) scenarios, at each running stage 250 GeV, 500 GeV, and 1 TeV, where the data at earlier stages is always combined to those at the current stage.

## 10. Summary and Acknowlegement

Figure 13 shows how well we will know about all Higgs couplings after the ILC baseline program. The physics case at the ILC is extremely compelling, and complementary to the LHC. A comprehensive and precision Higgs program without any model dependence offered by the ILC will be the key to reveal the secret of the EWSB and open the door to BSM physics.

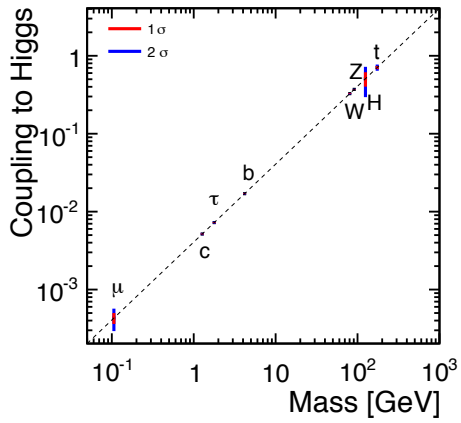


Figure 13: Expected mass-coupling plot after ILC baseline program. Error bars are shown for both 1 and 2 standard deviations.

Staged running is one great advantage to get best precisions, and capability of energy scan and beam polarisations can be really crucial if LHC rrun 2 would discover something new. Most importantly the ILC is technically ready to go [5, 6, 7, 8].

The authors would like to thank all the members of ILC physics subgroup and ILD and SiD detector optimization groups for useful discussions, especially to the colleagues working on the Higgs analyses, T. Barklow, M. Berggren, C. Calancha, C. Dürig, N. Graf, A. Ishikawa, S. Kawada, M. Kurata, A. Miyamoto, J. List, H. Ono, T. Price, P. Roloff, J. Strube, T. Suehara, T. Tanabe, S. Watanuki, R. Yonamine. The authors also would like to thank J. Strube for reading and helping improve the scripts. This work is supported in part by the Creative Scientic Research Grant No. 18GS0202 of the Japan Society for Promotions of Science (JSPS), the JSPS Grant-in-Aid for Science Research No. 22244031, and the JSPS Specially Promoted Research No. 23000002.

## References

[1] G. Aad, et al., Observation of a new particle in the search for the Standard Model Higgs boson with the ATLAS detector at the LHC, Phys.Lett. B716 (2012) 1–29. arXiv:1207.7214, doi:10.1016/j.physletb.2012.08.020.
[2] S. Chatrchyan, et al., Observation of a new boson at a mass of 125 GeV with the CMS experiment at the LHC, Phys.Lett. B716 (2012) 30–61. arXiv:1207.7235, doi:10.1016/j.physletb.2012.08.021.
[3] M. Peskin, Physics at the ILCTalk at the LCWS13.
[4] C. Brock, High Energy Frontier summary talk at Snowmass 2013.
[5] H. Baer, T. Barklow, K. Fujii, Y. Gao, A. Hoang, et al., The International Linear Collider Technical Design Report - Volume 2: PhysicsarXiv:1306.6352.
[6] C. Adolphsen, et al., The International Linear Collider Technical Design Report - Volume 3.I: Accelerator & in the Technical Design PhasearXiv:1306.6353.
[7] C. Adolphsen, et al., The International Linear Collider Technical Design Report - Volume 3.II: Accelerator Baseline DesignarXiv:1306.6328.
[8] T. Behnke, et al., The International Linear Collider Technical Design Report - Volume 4: DetectorsarXiv:1306.6329.
[9] D. Asner, T. Barklow, C. Calancha, K. Fujii, N. Graf, et al., ILC Higgs White PaperarXiv:1310.0763.
[10] H. Li, et al., HZ Recoil Mass and Cross Section Analysis in ILDarXiv:1202.1439.
[11] S. Watanuki, The study of precese measurement of Higgs recoil mass and cross section, and CP mixturePresentation at the LCWS14.
[12] M. Thomson, Hadronic recoil mass study at 350 GeVPresentation at the AWLC14.
[13] T. Tomita, Higgs recoil mass study in qqH channel at 250 GeV ILCPresentation at the LCWS14.
[14] T. Barklow, Using the Hadronic Recoil Cross Section Measurement in Higgs Coupling FitsPresentation at the LCWS14.
[15] A. Miyamoto, A measurement of the total cross section of $\sigma_{Zh}$ at a future $e^+e^-$ collider using the hadronic decay mode of ZarXiv:1311.2248.
[16] H. Ono, A. Miyamoto, A study of measurement precision of the Higgs boson branching ratios at the International Linear Collider, Eur.Phys.J. C73 (2013) 2343. arXiv:1207.0300, doi:10.1140/epjc/s10052-013-2343-8.
[17] J. Tian, et al., Determine the Higgs total width with $WW$-fusion production at ILC up to 500 GeVLC-REP-2013-022.
[18] T. Suehara, T. Tanabe, The LCFIPlus packageArticle in preparation.
[19] A. Ishikawa, Search for Invisible Higgs Decays at the ILCPresentation at the LCWS14.
[20] S.-i. Kawada, K. Fujii, T. Suehara, T. Takahashi, T. Tanabe, Full Simulation Study of the Higgs Branching Ratio into Tau Lepton Pairs at the ILC with $\sqrt{s}$ = 500 GeVarXiv:1403.7008.
[21] C. Calancha, Study of Higgs to $\gamma\gamma$ at 1 TeV at the ILCPresentation at the LCWS13.
[22] C. Calancha, Study of Higgs to $\mu^+\mu^-$ at 1 TeV at the ILCLC-REP-2013-006.
[23] M. E. Peskin, Estimation of LHC and ILC Capabilities for Precision Higgs Boson Coupling MeasurementsarXiv:1312.4974.
[24] J. Strube, Measurement of the Higgs Boson Coupling to the Top Quark and the Higgs Boson Self-coupling at the ILCProceedings of ICHEP14.
[25] R. Yonamine, et al., Measuring the top Yukawa coupling at the ILC at $\sqrt{s}$ = 500 GeV, Phys.Rev. D84 (2011) 014033. arXiv:1104.5132, doi:10.1103/PhysRevD.84.014033.
[26] T. Price, P. Roloff, J. Strube, T. Tanabe, Full simulation study of the top Yukawa coupling at the ILC at $\sqrt{s}$ = 1 TeVarXiv:1409.7157.
[27] J. Tian, et al., Study of Higgs self-coupling at the ILC based on full detector simulation at $\sqrt{s}$ = 500 GeV and $\sqrt{s}$ = 1 TeVLC-REP-2013-003.
[28] M. Kurata, et al., The Higgs Self Coupling Analysis Using The Events Containing $H \to WW^*$ DecayLC-REP-2013-025.
[29] C. Duerig, et al., Study of Higgs self-couplingPresentation at the AWLC14.
[30] G. P. Lepage, P. B. Mackenzie, M. E. Peskin, Expected Precision of Higgs Boson Partial Widths within the Standard ModelarXiv:1404.0319.
[31] M. E. Peskin, Comparison of LHC and ILC Capabilities for

Higgs Boson Coupling MeasurementsarXiv:1207.2516.
[32] T. Price, et al., Measurement of top Yukawa coupling at 1 TeV using ILD detectorLC-REP-2013-004.